AGU PUBLICATIONS

Radio Science

RESEARCH ARTICLE
10.1002/2013RS005307

Key Points:
- Development of an extended model for tracking error on GPS receivers
- It investigates the influence of the fading coefficients on the tracking error
- The model is used in a data set to predict the typical tracking error values

Correspondence to:
A. O. Moraes,
alisonaom@iae.cta.br

Citation:
Moraes, A. O., E. Costa, E. R. de Paula, W. J. Perrella, and J. F. G. Monico (2014), Extended ionospheric amplitude scintillation model for GPS receivers, *Radio Sci.*, *49*, 315–329, doi:10.1002/2013RS005307.

Received 26 SEP 2013
Accepted 9 APR 2014
Accepted article online 13 APR 2014
Published online 14 MAY 2014

Extended ionospheric amplitude scintillation model for GPS receivers

Alison de Oliveira Moraes[1], Emanoel Costa[2], Eurico Rodrigues de Paula[3], Waldecir João Perrella[4], and João Francisco Galera Monico[5]

[1]Instituto de Aeronáutica e Espaço—IAE, São José dos Campos, São Paulo, Brazil, [2]Centro de Estudos em Telecomunicações, Pontifícia Universidade Católica do Rio de Janeiro (CETUC/PUC-Rio), Rio de Janeiro, Rio de Janeiro, Brazil, [3]Instituto Nacional de Pesquisas Espaciais—INPE, São José dos Campos, São Paulo, Brazil, [4]Instituto Tecnológico de Aeronáutica—ITA, São José dos Campos, SP, Brazil, [5]Universidade Estadual Paulista Júlio de Mesquita Filho—UNESP, Presidente Prudente, Sao Paulo, Brazil

Abstract Ionospheric scintillation is a phenomenon that occurs after sunset, especially in the low-latitude region, affecting radio signals that propagate through the ionosphere. Depending on geophysical conditions, ionospheric scintillation may cause availability and precision problems to Global Navigation Satellite System users. The present work is concerned with the development of an extended model for describing the effects of the amplitude ionospheric scintillation on GPS receivers. Using the α-μ probabilistic model, introduced by previous authors in different contexts, the variance of GPS receiver tracking loop error may be estimated more realistically. The proposed model is developed with basis on the α-μ parameters and also considering correlation between amplitude and phase scintillation. Its results are interpreted to explain how a receiver may experience different error values under the influence of ionospheric conditions leading to a fixed scintillation level S_4. The model is applied to a large experimental data set obtained at São José dos Campos, Brazil, near the peak of the equatorial anomaly during high solar flux conditions, between December 2001 and January 2002. The results from the proposed model show that depending on the α-μ pair, moderate scintillation ($0.5 \le S_4 \le 0.7$) may be an issue for the receiver performance. When $S_4 > 0.7$, the results indicate that the effects of scintillation are serious, leading to a reduction in the receiver availability for providing positioning solutions in approximately 50% of the cases.

1. Introduction

Several environmental factors may affect GPS performance, such as electromagnetic interference, multipath, atmospheric delay, and fluctuations in signal amplitude and phase due to the ionosphere, respectively, known as amplitude and phase ionospheric scintillation. These fluctuations are due to diffraction of radio waves caused by kilometer-scale ionospheric plasma density irregularities [*Yeh and Liu*, 1982]. Ionospheric scintillation is responsible for significant deterioration in GPS accuracy that depending on its severity may even lead to a complete system failure [*Basu and Basu*, 1981; *Beach*, 1998]. Such phenomenon is more common in the low-latitude region (between approximately −20° and 20° geomagnetic latitude) and auroral and polar zones (above 55° of latitude) [*Jiao et al.*, 2013; *Mushini et al.*, 2011]. Additionally, scintillation activity that takes place after sunset has a temporal and seasonal dependence and follows the 11 year solar cycle in broad terms [*Kintner et al.*, 2004].

Scintillation affects the performance of GPS receivers notably at the signal tracking loop level. Depending on the scintillation level, there may be an increase in range measurement errors or even losses of lock of the carrier and code loops [*Kintner et al.*, 2001]. In extreme cases, scintillation can result in full disruption of the receiver operation [*Rezende et al.*, 2007].

Recently, *Moraes et al.* [2012, 2014] proposed and validated the use of the α-μ model to represent the amplitude and the second-order statistics of the GPS ionospheric scintillation phenomenon. This model was introduced by *Yacoub* [2007] and is based on two parameters, instead of just one, like those adopted in the literature [*Fremouw et al.*, 1980; *Rino*, 2011]. The results obtained by *Moraes et al.* [2012] indicated that the α-μ model is the most realistic in describing the amplitude scintillation among the tested distributions, basically due to the additional degree of freedom.

Conker et al. [2003] proposed a model for estimating the effects of amplitude scintillation on the availability of GPS receivers. This model assumed the Nakagami-*m* distribution for the statistical characterization of

amplitude scintillation. This assumption is based on the work of *Fremouw et al.* [1980], which showed that Nakagami-*m* distribution fitted well amplitude scintillation distributions. The present work, with foundations on the previous work of *Conker et al.* [2003], proposes an extended model for estimating the GPS receiver performance based on the α-μ distribution and derives the variances of the carrier and tracking loop errors of the GPS receiver. This extended model is based on a more realistic distribution for amplitude scintillation [*Moraes et al.*, 2012].

Section 2 presents in detail the α-μ distribution that will be used by the proposed models. The same section discusses the estimation of these coefficients and their physical interpretation, showing the benefits of α-μ distribution for modeling amplitude scintillation. Section 3 revisits the tracking error models for the GPS L1 receiver introduced by *Conker et al.* [2003] in the light of the α-μ distribution. The present extended model is explored, showing its mathematical restrictions and its advantages for performance estimations. Based on a large data set from the maximum of solar cycle 23, the typical error values that a user might expect under similar conditions are presented. Section 4 introduces the tracking error models for the GPS L2 aided by L1 receiver and shows the restrictions for the dual-frequency operation. Finally, section 5 presents concluding remarks.

2. The α-μ Distribution for Scintillation

The α-μ distribution is a general fading model introduced by *Yacoub* [2007]. Such a model is a version of the Stacy distribution [*Stacy*, 1962], rewritten in terms of fading parameters α and μ. The use of this distribution for modeling ionospheric amplitude scintillation was proposed by *Moraes et al.* [2012]. The probability density function of the normalized amplitude envelope r of the received signal, assuming that the resulting average signal power (or intensity) r^2 is equal to 1 (that is $E(r^2) = 1$), is given by

$$f(r) = \frac{\alpha r^{\alpha\mu-1}}{\xi^{\alpha\mu/2}\Gamma(\mu)} \exp\left(-\frac{r^\alpha}{\xi^{\alpha/2}}\right), \quad \xi = \frac{\Gamma(\mu)}{\Gamma(\mu + 2/\alpha)}, \tag{1}$$

where $\Gamma(.)$ is the gamma function. This model was originally applied to the characterization of the mobile communication channel under the assumption that the received signal results from a composition of clusters of multipath waves propagating in a nonhomogeneous environment [*Yacoub*, 2007]. It was also assumed that the random phases of the scattered waves have similar time delays within any cluster, with time delay spreads of different clusters being relatively large. The clusters of multipath waves were assumed to have components with identical powers. A nonlinear function of the modulus of the sum of contributions from these clusters of multipath components becomes the resulting envelope, where this nonlinearity is related to the power parameter α [*Yacoub*, 2002]. On the other hand, the μ parameter is the real and continuous extension to the number n of multipath components in the propagation environment. In other words, r^α is equal to the sum of n components of the type $\left(x_i^2 + y_i^2\right)$, where x_i and y_i are zero-mean, mutually independent Gaussian processes, and $i = 1, \ldots, n$. The probability density function obtained for r, which depends on α and n, is generalized by the substitution of μ (a real parameter) for n (an integer parameter). The details of the derivation of the α-μ distribution with basis on the above principles can be found in section 4 of *Yacoub* [2007].

An interesting feature of this general model is that it is able to accommodate several special cases. Depending on the values of its parameters, the α-μ distribution can become a Nakagami-*m* ($\alpha = 2$ and $\mu = m$, where m is the single parameter of the distribution), a Rayleigh ($\alpha = 2$ and $\mu = 1$), or a particular case of the Weibull distribution (with two parameters α and $\gamma = \xi^{1/2}$, for $\mu = 1$).

2.1. Amplitude Scintillation and Its Relation to the α-μ Coefficients

The S_4 index characterizes the severity of amplitude scintillation, and it is defined as the normalized standard deviation of the received signal intensity. It is given by [*Briggs and Parkin*, 1963]

$$S_4 = \sqrt{\frac{\langle I^2\rangle - \langle I\rangle^2}{\langle I\rangle^2}}, \tag{2}$$

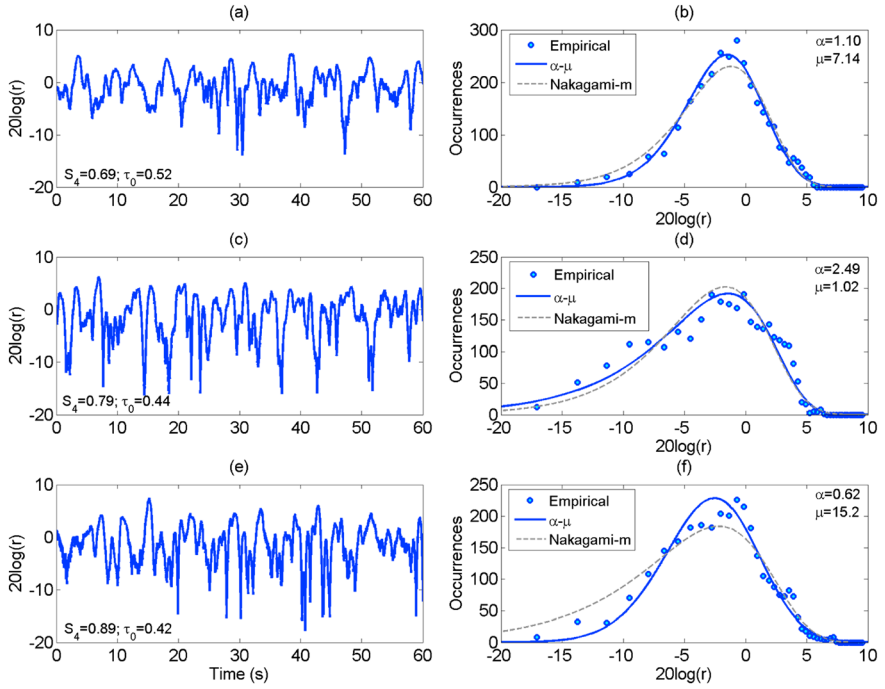

Figure 1. (a, c, and e) Three cases of amplitude scintillation categorized by the scintillation index S_4. (b, d, and f) Theoretical α-μ model based on the moment estimation of equation (4) in comparison with measured occurrences from Figures 1a, 1c, and 1e. The theoretical Nakagami-*m* probability density functions for the corresponding S_4 values are also shown.

where $I = |r|^2$ is the intensity of the received signal, and the angle brackets denote an ensemble average. The S_4 index is related to the *m* parameter of the Nakagami-*m* distribution by $m = 1/S_4{}^2$, where *m* may be estimated by the following relation between moments:

$$m = \frac{E^2(r^2)}{E(r^4) - E^2(r^2)}. \tag{3}$$

According to *Yacoub* [2007], the α and μ coefficients can be estimated with the basis on the equality:

$$\frac{E^2(r^\beta)}{E(r^{2\beta}) - E^2(r^\beta)} = \frac{\Gamma^2(\mu + \beta/\alpha)}{\Gamma(\mu)\Gamma(\mu + 2\beta/\alpha) - \Gamma^2(\mu + \beta/\alpha)}. \tag{4}$$

Ideally, the left-hand side of equation (4) can be obtained from field data for arbitrarily selected values of the parameter β, which indicates the order of the moment of the process *r* that should be evaluated. Taking $\beta = 1$ and $\beta = 2$ for example, and evaluating the left-hand side of equation (4) for a single-scintillation record, two equations with two unknowns are obtained. The numerical solution of this system of nonlinear equations, obtained through MATLAB's algorithm *fsolve*, provides the values of α and μ for the corresponding scintillation record. Exemplifying such an approach, Figure 1 provides, for different values of S_4, three cases of amplitude scintillation, where the α-μ model is successfully adjusted to experimental distributions with the basis on the moment equation (4). These cases were selected among the record of the field data described in more details in section 3.3.

There may be infinite (α, μ) values estimated for each value of the well-accepted and extensively used scintillation index S_4. This fact becomes more evident through a comparison of the left-hand side of equation (4) for $\beta = 2$ with the right-hand side of equation (2), making it is possible to establish the relationship:

$$S_4{}^2 = \frac{\Gamma(\mu)\Gamma(\mu + 4/\alpha) - \Gamma^2(\mu + 2/\alpha)}{\Gamma^2(\mu + 2/\alpha)}. \tag{5}$$

It can be shown, by making $\alpha = 2$ and using the properties of the gamma function, that the right-hand side of equation (5) reduces to $1/\mu = 1/m$ for the Nakagami-*m* distribution, as expected. It is convenient to have one model that describes different patterns of scintillation for the same scintillation index S_4. This is especially

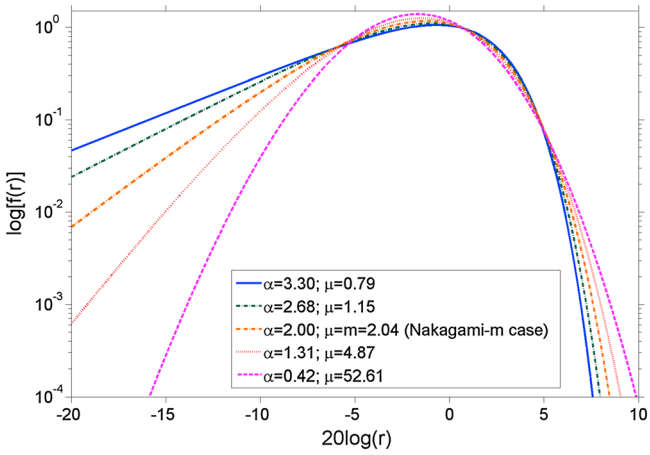

Figure 2. Various shapes of the α-μ probability density function, showing the relationship between the α coefficient and the severity of scintillation. For all curves, the considered scintillation index was $S_4 = 0.7$. When $\alpha = 2$, the α-μ model becomes the Nakagami-m distribution with $\mu = m$.

true for strong scintillation, where the S_4 index alone is not considered a proper indication of the ionospheric perturbations. Indeed, it saturates to a value near unity under increasingly strong scattering conditions, in addition to being independent of the rate of signal fading [*Carrano and Groves*, 2010]. With the aim at showing the influence of the (α, μ) parameters and their interpretation, Figure 2 illustrates five different shapes of the α-μ distribution for a fixed value of S_4 (=0.7), including the Nakagami-m case, where $\alpha = 2$ and $\mu = m = 1/S_4^2$. In this illustration, the curves vary substantially for the same S_4 value, that is for the same value on the left-hand side of equation (5). This flexibility of α-μ model, resulting from the existence of two parameters instead of just one, provides a better fit capacity to scintillation data. The values of α and μ, corresponding to each scintillation record, should be determined by the procedure described immediately below equation (4). It is worth mentioning that the distributions tend to spread as α increases, occupying the lower region of intensity values with higher probabilities. It means that the increased α values represent a more severe scenario for propagation, with a higher occurrence of deep fading of the received signal. For example, Figure 2 shows that the probability of fadings greater than 13 dB, corresponding to 20 log(r) < -13 dB (where 0 dB defines the unfaded signal level), is very small for $\alpha = 0.42$. On the other hand, a nonnegligible probability of fadings greater than 20 dB is observed for $\alpha = 3.30$. Indeed, a comparison between Figure 1c (with $S_4 = 0.79$ and $\alpha = 2.49$) and Figure 1e (with $S_4 = 0.89$ and $\alpha = 0.62$) indicates that the percentage of time that 20 log (r) < -10 dB is greater in the case with lower S_4 but higher α. This observation is confirmed by Figures 1d and 1f.

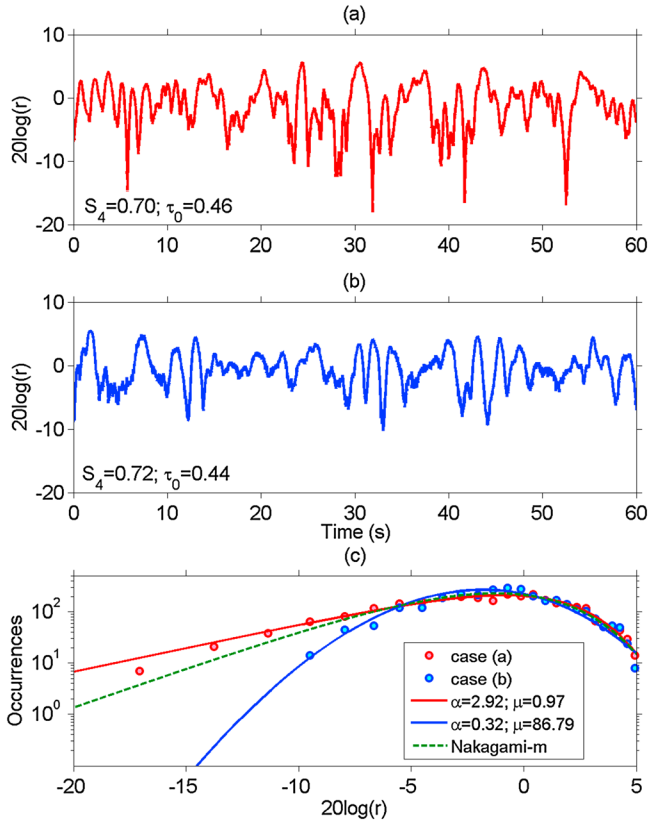

Figure 3. (a and b) Two cases illustrating the differences on the occurrences of the fades of equal depth for signals with approximately the same scintillation index S_4 and decorrelation time τ_o. (c) Corresponding measured occurrences and the α-μ distributions, as well as the Nakagami-m distribution with $m = 1/0.7^2 = 2.04$.

Extending the model interpretation, Figures 3a and 3b display two data set cases with very close values of the scintillation index S_4 and decorrelation time τ_o but with quite different (α, μ) coefficients, also estimated through equation (4). The decorrelation time τ_o is defined by $R_r(\tau_o)/R_r(0) = e^{-1}$, where $R_r(\tau)$ is the autocorrelation function of

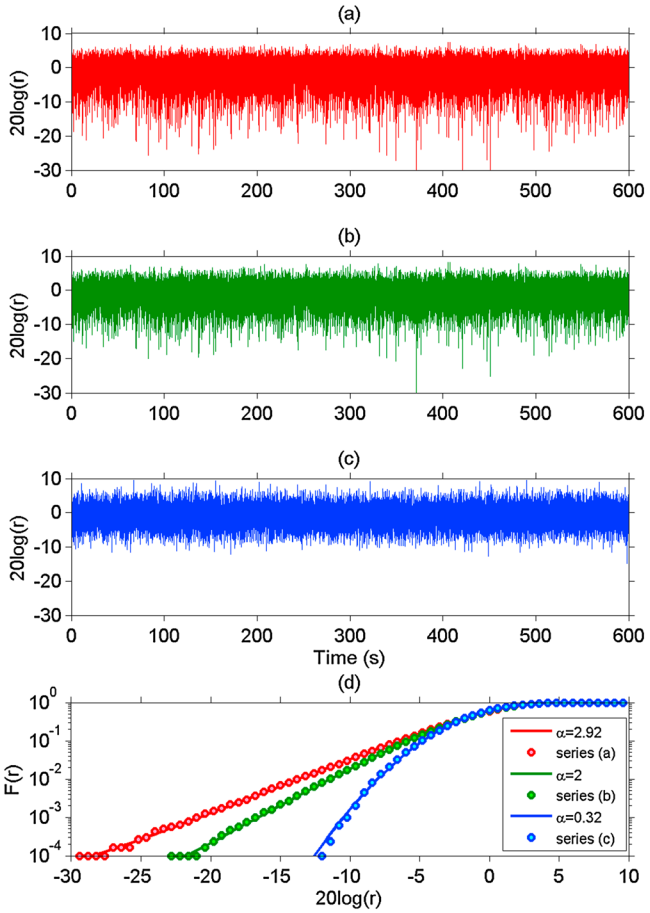

Figure 4. Simulated 10 min time series of random numbers conforming to the (a) α-μ distribution with $\alpha = 2.92$ and $\mu = 0.97$ (red), (b) Nakagami-*m* distribution with $m = 1/0.71^2 = 1.984$ (green), and (c) α-μ distribution with $\alpha = 0.32$ and $\mu = 86.79$ (blue). The same parameter values and color code of Figure 3 were used, respectively. All the simulated signals kept the same target value for S_4 (=0.71). (d) The respective target cumulative distribution functions (continuous curves), together with those resulting from the signals displayed in Figures 4a–4c, using hollow circles, are also shown.

r and $e \approx 2.718282$ is the Euler's number (base of the natural logarithm). The present cases were selected from the database described in section 3.3. Figure 3c compares the corresponding measured occurrences of selected signal power levels (circles) and the α-μ distributions, as well as the Nakagami-*m* distribution with $m = 1/0.7^2 = 2.04$. The differences between the distributions of these received signals, captured by the α-μ model, cannot be displayed by the single-parameter model. It could be argued that each of the 1 min data sets only contains a small number of deep fades. Thus, one could wonder if the displayed differences between the α-μ and the Nakagami-*m* could not be explained by sample variation. In response to this reasoning, Figures 4a–4c display the results from a simulation designed to generate 10 min time series of random numbers conforming to (a) the α-μ distribution with $\alpha = 2.92$ and $\mu = 0.97$ (red), (b) the Nakagami-*m* distribution with $m = 1/0.71^2 = 1.984$ (green), and (c) the α-μ distribution with $\alpha = 0.32$ and $\mu = 86.79$ (blue). Note that the same parameter values and color code of Figure 3 were used, respectively. All the simulated signals kept the same target value for S_4 (=0.71). Figure 4d shows the respective target cumulative distribution functions (continuous curves), together with those resulting from the signals displayed in Figures 4a–4c, using hollow circles. The four panels of Figure 4 clearly show that the probabilities of deep fades are very different for the three signals. Indeed, 10 realizations of the 10 min Nakagami-*m* signals were performed. The values of S_4 and of the probabilities associated with 10 dB and 15 dB fades varied in the respective intervals (0.696, 0.718), (0.0178, 0.0199), and (0.00156, 0.00234). That is, the differences between the α-μ and the Nakagami-*m* distributions observed in Figure 4d are far greater than those resulting from sample variation. In summary, the results from the simulation supports the discussion associated with Figures 1–3.

Another important aspect of this model is the relationship between the α and μ coefficients for a fixed value of the scintillation index S_4. Figure 5, prepared with the basis on equation (5), illustrates this relationship. It is seen that for each fixed value of S_4, an increase in the value of α implies a decrease in the μ coefficient, and vice versa. Considering the relation between these coefficients and the fundamental role of the index S_4 in scintillation studies, the analysis that follows will be mainly based on the pair of parameters (S_4 and α). The μ value corresponding to each pair can be immediately obtained from equation (5) or Figure 5 if necessary or desired. Of course, a similar analysis could be done using the pair of parameters (S_4 and μ), but the fact that $\alpha = 2$ turns the α-μ into the Nakagami-*m* distribution makes the focus on α more interesting and intuitive.

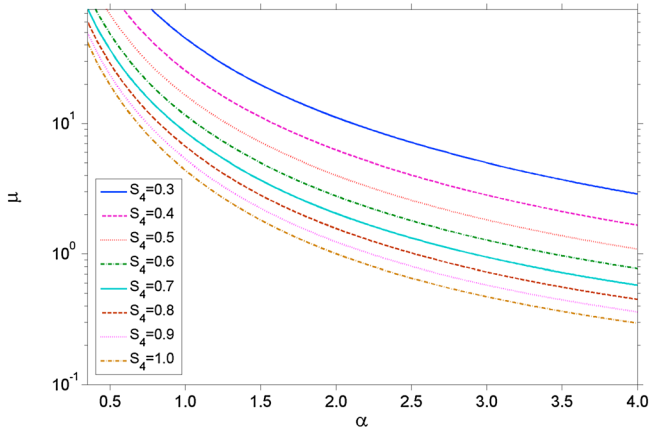

Figure 5. The α-μ relation for fixed values of the scintillation index S_4. Note that μ decreases as α increases to satisfy equation (5).

The relation expressed by equation (5) is also useful for theoretical works or when empirical data are not available. In such cases, it is necessary to know the (α, μ) values that will satisfy equation (5) for each value of S_4 and, most importantly, that best represent the distribution of amplitude scintillation. This second condition was enforced by the application of χ^2 tests to experimental data. *Moraes et al.* [2012] conducted a sequence of such tests to empirically obtain the parameters α and μ for the application of the α-μ model as a function of scintillation index S_4. Based on the above principles, the following approximation that yielded excellent results was proposed:

$$\hat{\alpha} = -17.649S_4{}^3 + 39.109S_4{}^2 - 27.8218S_4 + 7.498, \quad (6)$$

where $\hat{\alpha}$ is the approximate value of α. The corresponding μ value can be found by replacing $\hat{\alpha}$ for α in equation (5). Figure 6 illustrates various shapes of the α-μ probability density function based on the approximation of equation (6) for S_4 values ranging from 0.4 up to 1.0.

3. Effects of Ionospheric Scintillation for the GPS L1 Receiver

3.1. Carrier Tracking Loop

Scintillation affects phase tracking loops by increasing the phase error variance $\sigma^2_{\phi\varepsilon}$, decreasing the average time between cycle slips T_s, and ultimately causing frequency unlock. These related effects have been analyzed by different approaches.

One statistical model [*Conker et al.*, 2003] combined the scintillation index S_4 and the parameters of the phase spectral density to estimate $\sigma^2_{\phi\varepsilon}$. This model assumed loop operation in the linear regime and neglected any correlation between errors due to amplitude and phase scintillation. It also assumed that a receiver would reach a critical operation point whenever $\sigma^2_{\phi\varepsilon}$ exceeded a certain threshold. In addition, $\sigma^2_{\phi\varepsilon}$ was functionally related to T_s, assuming an unstressed first-order Costas loop. *Conker et al.* [2003] acknowledged that higher-order loops generally exhibit much smaller (2 to 3 orders of magnitude) values of T_s than those provided by the above relationship.

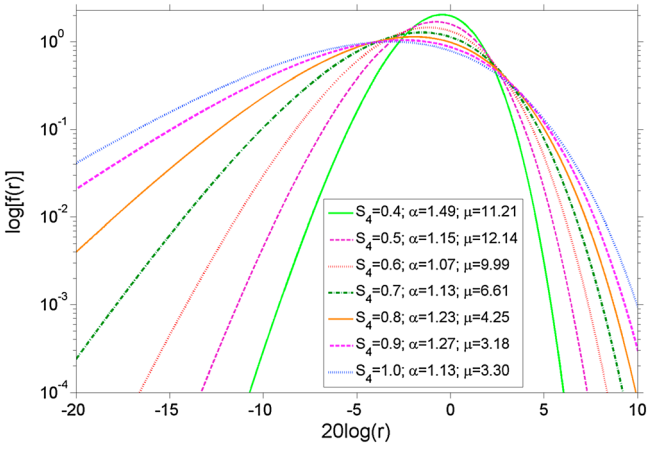

Figure 6. The α-μ probability density as a function of scintillation severity based on the parameterization of equation (6) for different values of S_4.

Humphreys et al. [2009, 2010a, 2010b] developed a flexible data-driven simulation test bed for evaluating the performance of carrier phase tracking loops. This model is based on a carefully preprocessed library of empirical phase and amplitude time series recorded under a wide range of equatorial scintillation conditions. The most striking features of the library are the power fades that are deeper than roughly 15 dB and occur simultaneously with abrupt, approximately half-cycle phase

changes. Test bed results showed that these canonical fadings accounted for over 90% of scintillation-induced cycle slips. When only amplitude fades or phase changes were retained, the cycle slipping rate decreased to less than 10% or roughly 50% of the native rate, respectively. Since no simplifying assumptions were introduced, this model can be considered to be very realistic even in the nonlinear regime. However, it is computationally expensive. Simulation tests performed by *Humphreys et al.* [2010b] also indicated that the mean time between bit errors T_e for differential phase shift keying detection could be used as a bound for T_s (on average, $T_s/2 < T_e < T_s$) for a particular phase-locked loop (PLL) type. Thus, using T_e as a rough proxy for T_s, a simple model for the latter parameter was developed, based on the scintillation index S_4, the complex scintillation signal decorrelation time τ_o, and the nominal carrier-to-noise ratio C/N_0.

Here the statistical model proposed by *Conker et al.* [2003] will be extended, with the basis on the α-μ distribution and also considering that errors due to amplitude and phase scintillation are correlated. The tracking error variance $\sigma^2_{\phi\varepsilon}$ at the output of the PLL is expressed by

$$\sigma^2_{\phi\varepsilon} = \sigma^2_{\phi S} + \sigma^2_{\phi T} + \sigma^2_{\phi osc} + 2\rho\sigma_{\phi S}\sigma_{\phi T}. \tag{7}$$

In the above equation, $\sigma^2_{\phi S}$ corresponds to the phase scintillation error component, $\sigma^2_{\phi T}$is the thermal noise component, $\sigma^2_{\phi osc}$ is related with the receiver oscillator noise, and ρ is the correlation coefficient between errors due to amplitude and phase scintillation. The receiver oscillator noise is a stationary random process independent from amplitude and phase scintillation, assumed to have a typical standard deviation of 0.015 rad. Note that equation (7) is exact, and the variances in its right-hand side can be calculated from the corresponding marginal distributions. Thus, previous results based on these marginal distributions can be used as starting points for the present development, which accepts the limitations described in the initial paragraphs of the current section. In particular, it neglects multipath effects, assumes operation in the linear regime, and that a receiver will reach a critical operation point whenever $\sigma\phi\varepsilon$ exceeds a certain threshold. *Humphreys et al.* [2010b] indicated that a squaring loop behaves approximately (within 20%) in the linearly regime for $\sigma\phi\varepsilon < 14.3°$.

The effect of phase scintillation on the tracking error variance at the output of the carrier loop is given by [*Conker et al.*, 2003]

$$\sigma^2_{\phi S} \cong \frac{\pi T}{k f_n^{p-1} \sin\left(\frac{(2k+1-p)\pi}{2k}\right)}, \tag{8}$$

where T and p are the spectral strength of the phase scintillation power spectral density (PSD) at 1 Hz and its slope, respectively. The parameters f_n and k are related to the PLL, where k is the order of the loop and f_n is the loop natural frequency in hertz. Equation (8) is valid for $1 < p < 2k$.

In the absence of scintillation, the component of the tracking error due to thermal noise in a PLL is given by [*Hegarty et al.*, 2001]

$$\sigma^2_{\varphi T} = \frac{B_n}{c/n_0}\left(1 + \frac{1}{2\eta c/n_0}\right), \tag{9}$$

where B_n is the PLL single-sided noise equivalent bandwidth, c/n_0 is the nominal carrier to noise density ratio for the coarse/acquisition (C/A) code L1 carrier, and η is the predetection integration period. In the present paper, the c/n_0 ratio is expressed in linear units (Hz), while C/N_0 expresses the same ratio in logarithmic units (dB Hz). It should be remarked that amplitude scintillation degrades the C/N_0 ratio, increasing the tracking error due to the thermal noise. Under this new condition, the PLL thermal noise tracking error can be represented by [*Conker et al.*, 2000]

$$\sigma^2_{\phi T} = \int_0^\infty \sigma^2_{\phi T}(r) f(r)\, dr, \tag{10}$$

where $\sigma^2_{\phi T}(r)$ results from the substitution of $r^2(c/n_0)$ for c/n_0 in equation (9) and $f(r)$ is defined by equation (1). Therefore, equation (10) becomes

$$\sigma^2_{\phi T} = \int_0^\infty \frac{B_n}{r^2 c/n_0}\left(1 + \frac{1}{2\eta r^2 c/n_0}\right)\frac{\alpha r^{\alpha\mu-1}}{\xi^{\alpha\mu/2}\Gamma(\mu)} e^{-r^\alpha/\xi^{\alpha/2}} dr. \tag{11}$$

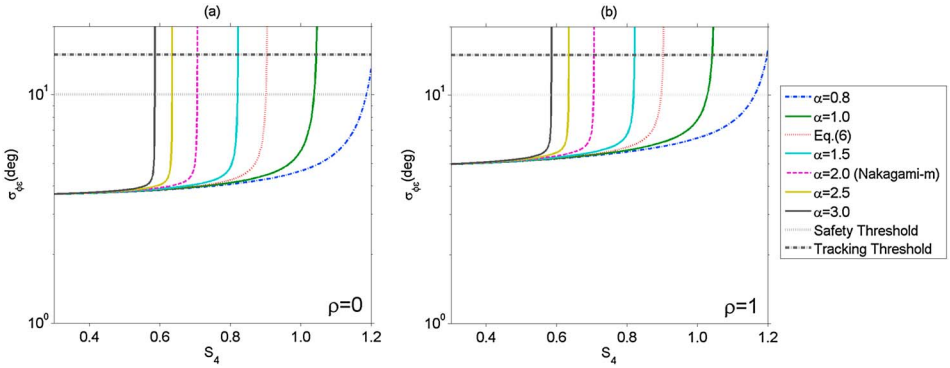

Figure 7. Standard deviation of the PLL tracking error as a function of the scintillation index S_4 for different values of α, based on the model of equations (7), (8), and (12). For $\alpha = 2$, this model is represented by equation (13). For the blue solid line, the values of α vary according to the polynomial approximation described by equation (6). These examples assumed $T = 0.005$ rad^2/Hz, $p = 2.5$, $f_n = 1.91$ Hz, $k = 3$, $C/N_0 = 42$ dBHz, $B_n = 15$ Hz, and $\eta = 1$ ms. (a) The curves assume no correlation ($\rho = 0$) between errors due to amplitude and phase scintillation. (b) The curves assume maximum correlation ($\rho = 1$). The tracking and safety thresholds are also plotted.

Thus, the thermal noise tracking error can be characterized in terms of the parameters α and μ according to the expression:

$$\sigma^2_{\phi T} = \frac{B_n}{c/n_0\,\xi\,\Gamma(\mu)}\left(\Gamma(\mu - 2/\alpha) + \frac{\Gamma(\mu - 4/\alpha)}{2\eta c/n_0\,\xi}\right). \tag{12}$$

Depending on the scintillation severity and also on the estimated α-μ parameters, the term $\sigma^2_{\phi T}$ in equation (7) may substantially contribute to or even become the major factor in the PLL tracking error variance. As mentioned in section 2, the α-μ parameters that are present in equation (12) may be obtained from field data with the help of equation (4). The results can then be used in equation (12) to estimate the tracking error caused by scintillation. When no field data are available, different approaches may be adopted. For example, the approximation of equation (6) that parameterizes the α and μ values as functions of scintillation index S_4 may be useful, since it is based on empirical data. Another possibility is the assumption of a constant value for α. It is important to remember in this assumption that higher α values are associated with also higher probabilities of deep fadings. Based on this assumption and taking $\alpha = 2$, it is seen that equation (12) includes the model by *Conker et al.* [2003], based on the Nakagami-*m* distribution with $m = 1/S_4{}^2$, as a special case:

$$\sigma^2_{\phi T} = \frac{B_n}{c/n_0\left(1 - S_4^2\right)}\left(1 + \frac{1}{2\eta(c/n_0)\left(1 - 2S_4^2\right)}\right). \tag{13}$$

The estimation based on equation (13) is valid only for $S_4 < 1/\sqrt{2}$. So it is not suitable for estimating the receiver performance under stronger scintillation conditions. On the other hand, the estimation based on equation (12) is more general, and the restriction on this model depends on the pair of α and μ values used in the argument of the gamma function $\Gamma(\mu - 4/\alpha)$, which must be greater than 0. Figure 7 shows the standard deviation of the tracking error $\sigma\phi\varepsilon$ represented by equations (7), (8), and (12) as a function of S_4, for fixed values of the parameters $T = 0.005$ rad^2/Hz, $p = 2.5$, $f_n = 1.91$ Hz [*Conker et al.*, 2003], $k = 3$, $C/N_0 = 42$ dBHz, $B_n = 15$ Hz, and $\eta = 1$ ms. The values for the parameters T and p resulted from recent processing of data from a Septentrio PolaRX scintillation monitor operated during February 2012 in São José dos Campos, Brazil, at the southern crest of the equatorial anomaly. This receiver is part of the Concept for Ionospheric Scintillation Mitigation for Professional Global Navigation Satellite System (GNSS) in Latin America network [http://cigala.galileoic.org]. To minimize tropospheric scattering and multipath effects, only data from GPS satellites with elevations greater than 30° were considered in our analyses. Power density spectral analysis of phase data was performed, providing maximum values $T_{max} = 0.0245$ rad^2/Hz and $p_{max} = 3.39$, as well as average values $T_{avg} = 0.001$ rad^2/Hz and $p_{avg} = 2.24$ for the parameters, respectively. Note that the assumed values are consistent with the experimental results. Most of the curves are labeled with the constant value assumed for α. Additionally, the curve that corresponds to the estimation of α based on equation (6) is also presented. For these curves, the corresponding μ values are obtained from the solution of equation (5) for the S_4 values.

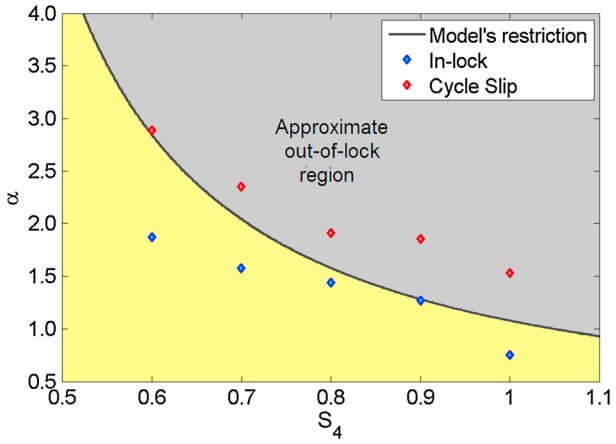

Figure 8. Restriction on the model of equation (12) as a function of scintillation index S_4 and the parameter α. The average values of α resulting from experimental data for selected values of S_4 are shown for in-lock and cycle slip cases.

This illustration also includes the case $\alpha = 2$, which transforms equation (12) into equation (13). The curves displayed in Figure 7a assume no correlation ($\rho = 0$) between errors due to amplitude and phase scintillation [*Conker et al.*, 2003]. Those curves in Figure 7b assume maximum correlation ($\rho = 1$) between the same error components. It is observed that all the curves start at $S_4 = 0.3$ with a small-slope section and end with an essentially vertical asymptotic branch. Changing the correlation coefficient from $\rho = 0$ to $\rho = 1$ raised the $\sigma\varphi\varepsilon$ values in the first section from approximately 3.7° to 5.0° but had virtually no effect on the asymptotic S_4 value for each curve. A study of equation (7) indicates that the asymptotic value is mainly defined by the standard deviation of the thermal noise component $\sigma\phi T$, characterized by equation (12). It is interesting to observe that the curves corresponding to $\rho = 0$ and $0.8 \le \alpha \le 1.5$, including the one based on equation (6), approximately span the same region with simulation results displayed in Figure 4 in the paper of *Humphreys et al.* [2010b]. In particular, the curve corresponding to $\rho = 0$ and $\alpha = 0.8$ provides a good fit to the simulation results associated with the GPS data (filled circles in Figure 4 of the above reference).

In the receiver loop, there exists a tracking threshold point in the evaluation of receiver performance, indicating where the loop stops working stably. When it happens, the error measurements become meaningless, the number of cycle slips increases drastically, and the receiver ultimately loses lock. The exact point of this transition and the dynamics of these related processes are hard to be determined. A reasonable value to be assumed as a threshold is $\sigma_{\phi\varepsilon} = 15°$, according to *Holmes* [1982] and *Ward et al.* [2006]. This threshold is consistent with the one indicated by *Humphreys et al.* [2010b], quoted above. *Conker et al.* [2003] suggested a safe threshold of 10° for aeronautical users, which represents a mean time to lose lock of about 3 h. Figure 7 also displays both tracking thresholds. It is observed that the tracking threshold and the safety threshold are exceeded by a lower level of scintillation as α increases. Indeed, these thresholds are almost coincident with the validity limit of equation (12). Therefore, it is reasonable to assume that the validity limit is also a stress point indicator for the receiver operation and performance, beyond which an out-of-lock condition will most likely be experienced. Figure 8 plots the restriction for the model described by equation (12) as a function of α and S_4. A different processing was also applied to the same Septentrio PolaRX data. Each individual channel of the receiver has a counter that resets at every loss-of-lock event. For each minute of intense scintillation, the parameters S_4, α, and μ were estimated. Each 1 min data record was classified according to the S_4 value and the absence (or presence) of counter resets. The presence of counter resets, extremely rare for $S_4 < 0.55$, was taken as an indication of occurrences of cycle slips. The average values of α were determined for the S_4 intervals (0.55, 0.65), (0.65, 0.75),…, and (0.95, 1.05), considering only records without counter resets. Next, the procedure was repeated for the remaining records (with counter resets). It is observed that the continuous restriction curve in Figure 8 yielded by the model successfully separates the two sets of average results (labeled as in-lock and cycle slip, respectively). This figure indicates that as S_4 increases, even received signals represented by relatively smaller α values will severely affect the loop operation. For example, GPS receiver loops would be more susceptible to lose lock in the case of Figure 3a, which displays a larger number of deep fades, than in the case of Figure 3b.

Figure 9 further illustrates the differences between the proposed α-μ and the Nakagami-*m* based models, described by equations (12) and (13), respectively. The standard deviation of the PLL thermal tracking error $\sigma_{\phi T}$ is plotted as a function of the C/N_0 ratio with parameters: (a) $S_4 = 0.7$, $B_n = 20$ Hz, and $\eta = 1$ ms and (b) $S_4 = 0.58$, $B_n = 15$ Hz, and $\eta = 3$ ms. Again, the safety and tracking thresholds are plotted. These plots also show

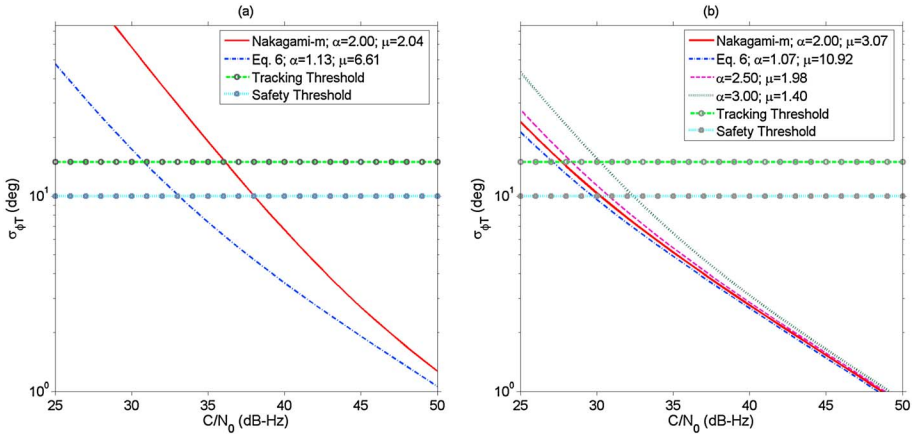

Figure 9. Comparison between the values of the standard deviation of the PLL thermal tracking error $\sigma_{\phi T}$ resulting from the α-μ and Nakagami-m ($\alpha = 2$ and $m = \mu = 1/S_4^2$) models, described by equations (12) and (13), respectively, for (a) $S_4 = 0.70$, $B_n = 20$ Hz, and $\eta = 1$ ms and (b) $S_4 = 0.57$, $B_n = 15$ Hz, and $\eta = 3$ ms. For the two plots, the values of α associated with the blue curves were estimated from those for S_4 using equation (6). Figure 9b also displays curves for $\alpha = 2.5$ and $\alpha = 3.0$. Except for the Nakagami-m curves, the μ values were obtained from equation (5) using the corresponding values for α and S_4.

the important role of the C/N_0 ratio in the tracking performance and how this ratio, allied with scintillation, may degrade the receiver performance.

3.2. Code Tracking Loop

According to *Conker et al.* [2003] and *Davies* [1990], a noncoherent delay-locked loop (DLL) is not affected by the phase scintillation. Therefore, the variance of the tracking error code delay at the output of the DLL is represented by $\sigma^2_{\tau\varepsilon} = \sigma^2_{\tau T}$, where $\sigma^2_{\tau T}$ is the variance of the thermal noise component. In the absence of scintillation, the variance of the DLL tracking error code loop as a function of the C/N_0 ratio is given by [*Hegarty*, 1997; *Conker et al.*, 2003]

$$\sigma^2_{\tau\varepsilon} = \sigma^2_{\tau T} = \frac{B_n d}{2c/n_0}\left(1 + \frac{1}{\eta c/n_0}\right), \tag{14}$$

where d is the correlator spacing in C/A chips.

It is immediate from a comparison between equations (9) and (14), in combination with the development of section 3.1, that the expressions for the variance of the DLL tracking error $\sigma^2_{\tau T}$ based on the α-μ or Nakagami-m distributions can be, respectively, obtained by straightforward multiplications of expressions (12) or (13) by $d/2$, together with the substitution of η for 2η in the denominators of the second terms within the outer pairs of parentheses. In particular,

$$\sigma^2_{\tau T} = \frac{B_n d}{2c/n_0 \Gamma(\mu)\xi}\left(\Gamma(\mu - 2/\alpha) + \frac{\Gamma(\mu - 4/\alpha)}{\eta c/n_0 \xi}\right). \tag{15}$$

The corresponding result by *Conker et al.* [2003], derived under the assumption of the Nakagami-m distribution, is obtained from equation (15) for the set of values $\alpha = 2$ and $m = \mu = 1/S_4^2$.

The restriction for the variance of the DLL tracking error $\sigma^2_{\tau\varepsilon}$, based on the α-μ distribution, is exactly the same as the one for equation (12) shown in Figure 8. Figure 10 displays $\sigma_{\tau\varepsilon(\text{meters})} = W_{C/A}\sigma_{\tau\varepsilon}$, where $W_{C/A}$ is the chip length of 293.0523 m, as a function of C/N_0. Figure 10a considers the case $S_4 = 0.70$, $d = 0.5$, $B_n = 1.0$ Hz, and $\eta = 3$ ms. For Figure 10b, the values are $S_4 = 0.58$, $d = 0.25$, $B_n = 0.5$ Hz, and $\eta = 5$ ms. The values of the tracking threshold for the DLL, which depend on $d/3$ [*Ward et al.*, 2006], are also plotted in Figure 10. As shown in Figure 9, it is possible to note that C/N_0 and the S_4 index play the major roles in the code loop performance.

3.3. Field Measurements and Performance Evaluation

This subsection explores the proposed model by direct application of the α-μ model to an experimental data set. The available measurements were made by a scintillation monitor developed by *Beach and Kintner*

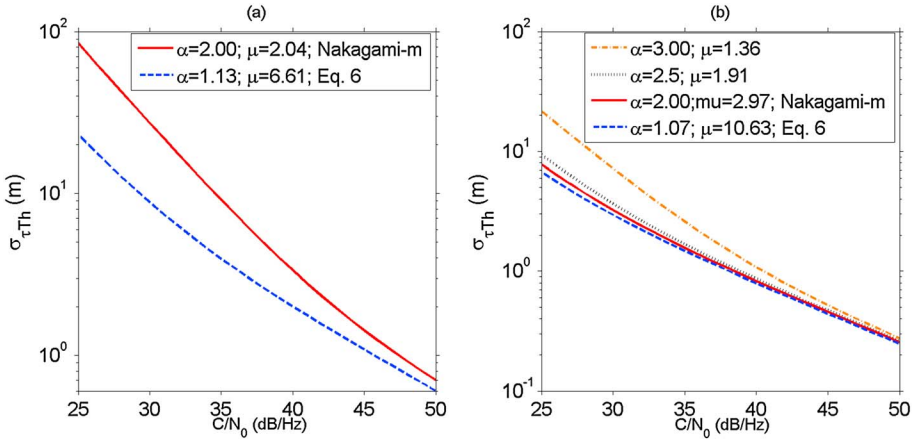

Figure 10. Comparison between the values of the standard deviation of the DLL thermal tracking error resulting from the α-μ and Nakagami-*m* ($\alpha = 2$) models for (a) $S_4 = 0.70$, $d = 0.5$, $B_n = 1.0$ Hz, and $\eta = 3$ ms and (b) $S_4 = 0.58$, $d = 0.25$, $B_n = 0.5$ Hz, and $\eta = 5$ ms. For the two plots, the values of α associated with the blue curves were estimated from those for S_4 using equation (6). Figure 10b also displays curves for $\alpha = 2.5$ and $\alpha = 3.0$.

[2001] and located under the equatorial anomaly peak in São José dos Campos, Brazil, during a period of high-solar activity between 14 December 2001 and 14 January 2002. A total of 3445 nonconsecutive records lasting 60 s each were obtained with a sample rate of 50 Hz during local evening hours. Each record corresponds to a time series of 3000 consecutive samples of received amplitude signals and to $S_4 \geq 0.3$. Details about these measurements and the corresponding data processing can be found in *Moraes et al.* [2011] and *Moraes et al.* [2012]. These references also compare the special Nakagami-*m* (when $\alpha = 2$) distribution and the approximation of equation (6) with the results based on the α-μ moment-based estimator.

Table 1 presents the typical error values computed with the basis on the above procedures assuming the fixed parameter values $C/N_0 = 42$ dB Hz, $\eta = 3$ ms, and $d = 0.5$ chip. The values $B_n = 15$ Hz and $B_n = 5$ Hz were assumed for noise equivalent bandwidths of the carrier and code loops, respectively. The results are classified according to the value of the scintillation index S_4 (for each column). The first line (labeled "Cases") indicates, for each S_4 value, the corresponding total number of 60 s records, immediately followed by the number of estimated α-μ pairs that do not meet the restriction criterion $\alpha\mu > 4$ of the α-μ model resulting from equations (12) and (15). For each S_4 value, the two numbers in the line labeled Cases are separated by a slash. Consequently, the receiver would be more vulnerable to the losses of lock, when the restriction criterion is violated and the associated average α values are reported in the line labeled "Out of lock" of Table 1. The average values of α (resulting from the application of equation (4) to experimental data), $\sigma_{\varphi T}$, and $\sigma_{\tau T}$ for the cases meeting the restriction criterion of the α-μ model (differences between the two figures in the line

Table 1. Comparison Between Carrier and Code Thermal Tracking Error Estimations by Different Methods[a]

Method	S_4	0.3	0.4	0.5	0.6	0.7	0.8	0.9	1.0
Cases		1395/0	726/0	479/15	330/39	217/64	139/61	116/60	43/22
Out of lock	E[α]	-	-	5.86	3.71	3.05	2.32	1.94	1.87
Equation (4)	E[α]	1.79	1.71	1.17	1.06	0.98	0.91	0.90	0.80
	E[$\sigma_{\varphi T}$] (deg)	1.85	1.92	2.01	2.15	2.32	2.56	3.22	3.29
	E[$\sigma_{\tau T}$] (m)	2.75	2.86	3.01	3.23	3.52	3.93	5.29	5.38
Equation (6)	$\hat{\alpha}$	2.19	1.49	1.15	1.07	1.13	1.23	1.27	1.13
	$\sigma_{\varphi T}$ (deg)	1.86	1.93	2.02	2.14	2.32	2.62	5.32	-
	$\sigma_{\tau T}$ (m)	2.76	2.87	3.01	3.20	3.49	4.02	10.29	-
Equation (13) Nakagami	(m)	11.11	6.25	4.00	2.77	2.04	1.56	1.23	1.00
	$\sigma_{\varphi T}$ (deg)	1.85	1.93	2.05	2.24	3.04	-	-	-
	$\sigma_{\tau T}$ (m)	2.76	2.88	3.06	3.37	5.21	-	-	-

[a]These cases assumed the fixed values $C/N_0 = 42$ dBHz, $\eta = 3$ ms, $d = 0.5$ chip, as well as $B_n = 15$ Hz and $B_n = 5$ Hz for the carrier and code loops, respectively.

labeled Cases) are shown in the next three lines labeled "Equation (4)." The values of $\sigma_{\varphi T}$ and $\sigma_{\tau T}$ are determined from the respective applications of equations (12) and (15) to the resulting α–μ pairs. The value of $\hat{\alpha}$ can be determined from equation (6) for each value of S_4. The corresponding μ value can be obtained from equation (5) or Figure 5, and the $\hat{\alpha} - \mu$ pair used to calculate the associated values of $\sigma_{\varphi T}$ and $\sigma_{\tau T}$ as before. The corresponding results are shown in the three lines labeled "Equation (6)." For the special Nakagami-*m* (when $\alpha = 2$) distribution, the values of all the parameters $m = 1/S_4^2$, $\sigma_{\varphi T}$, and $\sigma_{\tau T}$ can be directly determined from those of the associated S_4. For this special case, $\sigma_{\varphi T}$ and $\sigma_{\tau T}$ are calculated from equation (13) and from the particular version of equation (15) with $\alpha = 2$ and $\mu = m = 1/S_4^2$, respectively. The results are displayed in the last three lines labeled "Equation (13)."

It is interesting to observe the number of cases with α-μ pairs leading to a critical condition, labeled out-of-lock cases in Table 1. In relative terms, the number of these cases increases substantially with the scintillation index S_4: from 30% of the cases for $S_4 = 0.7$ to more than 50% for $S_4 \geq 0.9$. The average α values for these cases decreases with S_4, which was expected according to Figure 8.

Analyzing Table 1, one concludes that the results $\sigma_{\varphi T}$ and $\sigma_{\tau T}$ from the last two methods (displayed in the set of lines labeled Equation (6) and Equation (13)) are in good agreement with the corresponding results ($E[\sigma_{\varphi T}]$ and $E[\sigma_{\tau T}]$, respectively) from the use of the α-μ moments for weak to moderate scintillation (displayed in the set of lines labeled Equation (4)). However, the agreement breaks down for values of S_4 close to the validity limit of each of the two methods. It is noted that the approximation provided by equation (6) extends the agreement to a wider range than that resulting from the Nakagami-*m* model.

4. Effects of Ionospheric Scintillation on a Semicodeless GPS L2 Receiver

Dual-frequency receivers are extremely important for precision applications such as augmentation systems or others that involve differential techniques. This kind of receiver is mainly used to remove the ionospheric delay from the pseudorange, improving its accuracy. While the L1 frequency broadcasts the precise (P) and C/A codes, the L2 frequency broadcasts only the P code. When the antispoofing (AS) is activated by the control segment, a pseudo random number code, namely W, is inserted to generate the P(Y) code. When it happens, Standard Positioning Service users immediately lose the two frequency operation mode [*Ward et al.*, 2006]. However, there are many techniques to overcome this problem. The goal of these techniques is to use the carrier of GPS L1 to help reconstruct the L2 carrier phase under AS. They are known as codeless or semicodeless, depending if the user has some information or not about the W code. The main codeless and semicodeless techniques have been described by *Woo* [1999]. This section presents the models for the effects of scintillation on the GPS L2 semicodeless and code tracking loops. *Conker et al.* [2003] will again be the basis for the development in the present section.

4.1. Carrier Tracking Loop

Conker et al. [2003] derived a model for the PLL error variance of a semicodeless L2 receiver aided by L1, expressed in the same format of equation (7). For the phase scintillation element of L2, it is necessary to know the spectral strength T of the phase scintillation PSD at 1 Hz and its slope p from the phase of L1. These parameters are used together with the frequency factor $a = f_{L2}/f_{L1} = 60/77$ to produce the following result

$$\sigma_{\phi S2}^2 \cong \frac{\pi T}{k f_n^{p-1} \sin\left(\frac{(2k+1-p)\pi}{2k}\right)} \cdot \begin{cases} (a^2 + a^{-2}) & \text{case A} \\ (a^2 + a^{-2} - 2) & \text{case B} \end{cases}. \tag{16}$$

Equation (16), which is similar to equation (8), involves the frequency factor a in two cases: the first (A) assumes that the phase components of carrier frequency L1 and L2 are uncorrelated and the second (B) assumes full correlation between the phase components, taking $k = 2$ and $f_n = 0.075$ Hz, according to *van Dierendonck* [1996]. The analyses of the phase scintillation component or its correlation with the thermal error component, which are parts of equation (7), are not the main objectives of this section. The results below concern only the thermal errors due to scintillation. More details on this subject can be found in *Conker et al.* [2003].

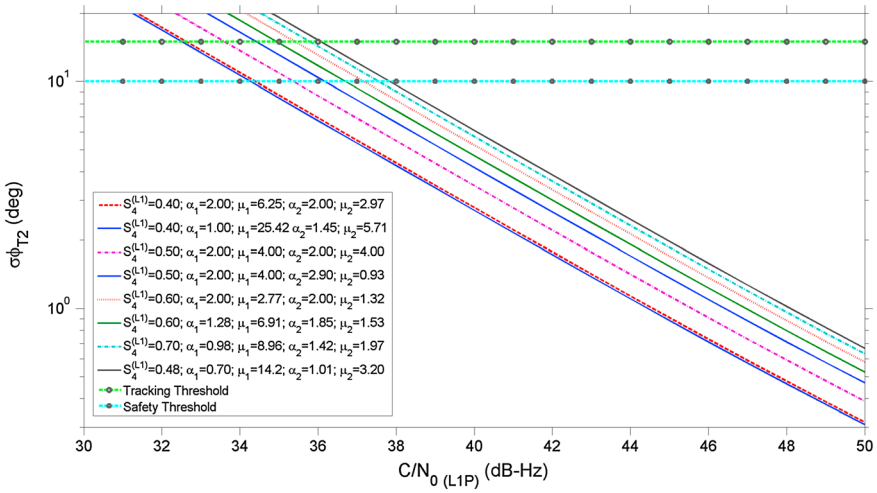

Figure 11. Standard deviation of thermal tracking error $\sigma_{\phi T2}$, for a semicodeless L2 receiver aided by L1, as a function of $(C/N_0)_{L1P}$ for various scenarios. In these examples, $B_n = 0.25$ Hz, $\eta_Y = 1.96$ μs, $S_4(L2) = 1.454\ S_4(L1)$, and $(C/N_0)_{L2P} = (C/N_0)_{L1P} - 3$ dB.

In the absence of scintillation, the tracking error variance due to the thermal noise component of a semicodeless L2 receiver aided by L1 is

$$\sigma^2_{\phi T2} = \frac{B_n}{(c/n_0)_{L2P}}\left(1 + \frac{1}{2\eta_Y (c/n_0)_{L1P}}\right). \tag{17}$$

In the above equation, $\eta_Y = 1.96$ μs is the GPS predetection time for the Y code on L2. However, the same variance, in the presence of scintillation, should be represented by

$$\sigma^2_{\phi T_2} = \int_0^\infty\int_0^\infty \sigma^2_{\phi T_2}(r_1, r_2) f(r_1, r_2)\, dr_1 dr_2 = \int_0^\infty\int_0^\infty \sigma^2_{\phi T_2}(r_1, r_2) f(r_1) f(r_2)\, dr_1 dr_2, \tag{18}$$

where $\sigma^2_{\phi T}2(r_1, r_2)$ results from the substitution of $r^2_{1,2}(c/n_0)_{L(1,2)P}$ for $(c/n_0)_{L(1,2)P}$ into equation (17). Scintillation on the L1 and L2 signals are assumed to be independent, allowing the joint probability density function $f(r_1,r_2)$ to be expressed by the product in the right-hand side of equation (18). A development based on the above equation and the α-μ model leads to

$$\sigma^2_{\varphi T2} = \frac{B_n \Gamma(\mu_2 - 2/\alpha_2)}{(c/n_0)_{L2P}\Gamma(\mu_2)\xi_2}\left(1 + \frac{\Gamma(\mu_1 - 2/\alpha_1)}{2\eta_Y (c/n_0)_{L1P}\Gamma(\mu_1)\xi_1}\right), \tag{19}$$

where $(c/n_0)_{L1P}$ and $(c/n_0)_{L2P}$ are the carrier to noise density ratios for the P code L1 and L2 carrier frequencies, α_1-μ_1 and α_2-μ_2 are the corresponding pairs of parameters, respectively, and $\xi_{1,2} = \Gamma(\mu_{1,2})/\Gamma(\mu_{1,2} + 2/\alpha_{1,3})$. It is also immediate that in the particular case of the Nakagami-*m* distribution with $\alpha_{1,2} = 2$ and $\mu_{1,2} = 1/S^2_4(L1, 2)$, the above equation is reduced to the result obtained by *Conker et al.* [2003]

$$\sigma^2_{\phi T2} = \frac{B_n}{(c/n_0)_{L2P}\left(1 - S^2_4(L2)\right)}\left(1 + \frac{1}{2\eta_Y (c/n_0)_{L1P}\left(1 - S^2_4(L1)\right)}\right). \tag{20}$$

In principle, this model would be valid for $S_4(L1,2) < 1$. However, according to *Hegarty et al.* [2001], the relation $S_4(L2) = 1.454\ S_4(L1)$ forces this model to be valid only for $S_4(L1) < 0.687$.

Figure 11 shows examples of $\sigma^2_{\phi T}$ as a function of $(C/N_0)_{L1P}$ for different combinations of parameters. In addition to the relation between the S_4 values at the two frequencies introduced in the previous paragraph, these example also assume $(C/N_0)_{L1P} \approx (C/N_0)_{L1\text{-}C/A} - 3$ dB and $(C/N_0)_{L2P} \approx (C/N_0)_{L1\text{-}C/A} - 6$ dB, according to *Conker et al.* [2003]. Once again, the model based on α-μ distribution is valid over wider range, depending on the α_2-μ_2 values in the argument of gamma function in the numerator of equation (19).

4.2. Code Tracking Loop

In the absence of scintillation, the variance of the DLL error due to noise or wideband interference, in chips square, for a semicodeless L2 receiver aided by L1 is [*Conker et al.*, 2003]

$$\sigma^2_{\tau T2} = \frac{B_n}{2(c/n_0)_{\mathrm{L2P}}}\left(1 + \frac{1}{2\eta_Y (c/n_0)_{\mathrm{L1P}}}\right), \tag{21}$$

where $B_n = 0.3$ Hz is the one-sided bandwidth. Note that equations (17) and (21) are related by the factor 0.5. Therefore, multiplication of equations (19) and (20) by the same factor immediately provides the results for $\sigma^2_{\tau T2}$ in the presence of scintillation, assuming the α-μ and the Nakagami-*m* models, respectively. The corresponding variances should be multiplied by the chip length (29.30523 m) to be expressed in meters. The behaviors of these results can be inferred from Figure 11.

5. Summary and Conclusions

This work derives a realistic and flexible model to calculate the effects of amplitude ionospheric scintillation on GPS receivers by applying the α-μ distribution to the fundamental expressions previously presented by *Conker et al.* [2003]. Indeed, the previous results, obtained under the assumption of the Nakagami-*m* distribution for the amplitude scintillation, are immediately obtained from the present ones in the particular case $\alpha = 2$. The extended model, which displays a broader validity range, was used to predict the variances of the tracking error in the receiver carrier and code loops. The tracking error values were estimated from real data by using the equality of moments of the α-μ distribution. The results were compared with the estimations based on the Nakagami-*m* distribution and a polynomial approximation that allows the use of the present model for theoretical works over a wide range of scintillation regimes. Estimations based on the experimental data indicate that in relative terms, the number of critical condition cases increase substantially with the scintillation index S_4. Additionally, the average α values for these cases decreases with S_4. One concludes that the results from the Nakagami-*m* distribution or the polynomial approximation for the relation between S_4 and α are in good agreement with the results from the extended model for weak to moderate scintillation. However, the agreement deteriorates or these two models break down for high values of S_4.

The present model neglects multipath effects, assumes operation in the linear regime, and that a receiver will reach a critical operation point whenever the standard deviation of the PLL phase error exceeds a certain threshold. It can be easily implemented and applied to configurations of interest. Within its validity limits (namely, $\sigma_{\phi c} < 14.3°$), the results are consistent with the ones provided by a flexible data-driven simulation test bed [*Humphreys et al.*, 2010b] for a similar configuration. It is also capable of successfully discriminating in-lock from cycle-slip situations, on average, in the presence of moderate to strong scintillation ($0.55 < S_4 > 1.05$). However, the present version of the model does not relate the standard deviation of the phase error to the average time between cycle slips T_s or predict the corresponding rate [*Humphreys et al.*, 2009, 2010a, 2010b].

The models for semicodeless receivers are also proposed. The results for these models confirm the dramatic decrease in the performance of L2 aided by L1 loops, as pointed out by *Hegarty et al.* [2001]. This is basically due to the short integration time and the lack of information about the Y code.

The models proposed here may be useful in a series of applications. For example, to improve the positioning accuracy for link weighted models [*Aquino et al.*, 2009] and the tracking jitter variance maps for GNSS availability [*Sreeja et al.*, 2011]. As shown in this paper, the α and μ values are capable of expressing the severity of scintillation, being complementary parameters in the scintillation analysis and the tracking loop models. Based on the α-μ model, a strategy for the mitigation of ionospheric effects on GNSS by using a network of continuously operating reference stations [*Yang et al.*, 2011] could also be developed.

Acknowledgments
The authors are grateful to Fabiano Rodrigues (University of Texas at Dallas, TX, USA) and Marcio Muella (Universidade do Vale do Paraíba, SP, Brazil) for the discussions concerning the application of the α-μ model for scintillation. A.O.M. wishes to thank the Instituto de Aeronáutica e Espaço, where he works as a research engineer, for supporting and assisting his cooperation research with INPE and ITA. E.C. was supported by AFOSR award FA9550-12-1-0031 during the present work. E.R.P. is grateful for the partial supports from AFOSR FA9550-10-1-0564 and CNPq 305684/2010-8 grants. J.F.G.M. thanks the support from FAPESP through award 2006/04008-2 and Galileo FP7 R&D program. The authors also thank the reviewers for the insightful and constructive comments, which helped them in the development of a better paper.

References

Aquino, M., J. Monico, A. Dodson, H. Marques, G. De Franceschi, L. Alfonsi, V. Romano, and M. Andreotti (2009), Improving the GNSS positioning stochastic model in the presence of ionospheric scintillation, *J. Geod.*, *83*, 953–966, doi:10.1007/s00190-009-0313-6.
Basu, S., and S. Basu (1981), Equatorial scintillations - A review, *J. Atmos. Sol. Terr. Phys.*, *43*, 473–489.
Beach, T. L. (1998), Global Positioning System studies of equatorial scintillations, PhD thesis, Cornell University.

Beach, T. L., and P. M. Kintner (2001), Development and use of a GPS ionospheric scintillation monitor, *IEEE Trans. Geosci. Remote Sens.*, *39*, 918–928, doi:10.1109/36.921409.

Briggs, B. H., and I. A. Parkin (1963), On the variation of radio star and satellite scintillations with zenith angle, *J. Atmos. Terr. Phys.*, *25*, 339–366, doi:10.1016/0021-9169(63)90150-8.

Carrano, C. S., and K. M. Groves (2010), Temporal decorrelation of GPS satellite signals due to multiple scattering from ionospheric irregularities. Proc. of the 2010 Institute of Navigation ION GNSS meeting, Portland, OR, Institute of Navigation, 361–374.

Conker, R. S., M. B. El-Arini, C. J. Hegarty, and T. Hsiao (2000), Modeling the effects of ionospheric scintillation on GPS/WAAS availability, Rep. MP00W179, The MITRE Corp., McLean, Va.

Conker, R. S., M. B. El-Arini, C. J. Hegarty, and T. Hsiao (2003), Modeling the effects of ionospheric scintillation on GPS/Satellite-Based Augmentation System availability, *Radio Sci.*, *38*(1), 1001, doi:10.1029/2000RS002604.

Davies, K. (1990), *Ionospheric Radio*, IEE Electromagnetic Waves Series, Peter Peregrinus Ltd., London, U. K.

Fremouw, E. J., R. C. Livingston, and D. A. Miller (1980), On the statistics of scintillating signals, *J. Atmos. Sol. Terr. Phys.*, *42*, 717–731.

Hegarty, C. J. (1997), Analytical derivation of maximum tolerable inband interference levels for aviation applications of GNSS, *Navigation*, *44*(1), 25–34.

Hegarty, C., M. B. El-Arini, T. Kim, and S. Ericson (2001), Scintillation modeling for GPS-Wide Area Augmentation System receivers, *Radio Sci.*, *36*, 1221–1231.

Holmes, J. K. (1982), *Coherent Spread Spectrum Systems*, John Wiley, New York.

Humphreys, T. E., M. L. Psiaki, J. C. Hinks, B. O'Hanlon, and P. M. Kintner Jr. (2009), Simulating ionosphere-induced scintillation for testing GPS receiver phase tracking loops, *IEEE J. Sel. Top. Signal Process.*, *3*(4), 707–715.

Humphreys, T. E., M. L. Psiaki, B. M. Ledvina, A. P. Cerruti, and P. M. Kintner Jr. (2010a), Data-driven testbed for evaluating GPS carrier tracking loops in ionospheric scintillation, *IEEE Trans. Aerosp. Electron. Syst.*, *46*(4), 1609–1623.

Humphreys, T. E., M. L. Psiaki, and P. M. Kintner (2010b), Modeling the effects of ionospheric scintillation on GPS carrier phase tracking, *IEEE Trans. Aerosp. Electron. Syst.*, *46*(4), 1624–1637.

Jiao, Y., Y. T. Morton, S. Taylor, and W. Pelgrum (2013), Characterization of high-latitude ionospheric scintillation of GPS signals, *Radio Sci.*, *48*, 698–708, doi:10.1002/2013RS005259.

Kintner, P. M., H. Kil, T. L. Beach, and E. R. de Paula (2001), Fading timescales associated with GPS signals and potential consequences, *Radio Sci.*, *36*, 731–743, doi:10.1029/1999RS002310.

Kintner, P. M., B. M. Ledvina, E. R. de Paula, and I. J. Kantor (2004), Size, shape, orientation, speed, and duration of GPS equatorial anomaly scintillations, *Radio Sci.*, *39*, RS2012, doi:10.1029/2003RS002878.

Moraes, A. O., F. S. Rodrigues, W. J. Perrella, and E. R. Paula (2011), Analysis of the characteristics of low-latitude GPS amplitude scintillation measured during solar maximum conditions and implications for receiver performance, *Surv. Geophys.*, *33*(5), 1107–1131, doi:10.1007/s10712-011-9161-z.

Moraes, A. O., E. R. Paula, W. J. Perrella, and F. S. Rodrigues (2012), On the distribution of GPS signal amplitudes during the low-latitude ionospheric scintillation, *GPS Solutions*, doi:10.1007/s10291-012-0295-3.

Moraes, A. O., E. R. de Paula, M. T. de Assis Honorato Muella, and W. J. Perrella (2014), On the second order statistics for GPS ionospheric scintillation modeling, *Radio Sci.*, *49*, 94–105, doi:10.1002/2013RS005270.

Mushini, S. C., P. T. Jayachandran, R. B. Langley, J. W. MacDougall, and D. Pokhotelov (2011), Improved amplitude- and phase-scintillation indices derived from wavelet detrended high-latitude GPS data, *GPS Solutions*, *16*, 363–373.

Rezende, L. F. C., E. R. de Paula, I. J. Kantor, and P. M. Kintner (2007), Mapping and survey of plasma bubbles over Brazilian territory, *J. Navig.*, *60*, 69–81.

Rino, C. (2011), *The Theory of Scintillation with Applications in Remote Sensing*, Wiley-IEEE Press, Hoboken, N. J.

Sreeja, V., M. Aquino, and Z. G. Elmas (2011), Impact of ionospheric scintillation on GNSS receiver tracking performance over Latin America: Introducing the concept of tracking jitter variance maps, *Space Weather*, *9*, S10002, doi:10.1029/2011SW000707.

Stacy, E. W. (1962), A generalization of the gamma distribution, *Ann. Math. Stat.*, *33*(3), 1187–1192.

Van Dierendonck, A. J. (1996), GPS Receivers, in *Global Positioning System: Theory and Applications*, chap. 8, edited by B. Parkinson and J. J. Spilker Jr., pp. 329–405, AIAA, Inc., Washington, D. C.

Ward, P. W., J. W. Betz, and C. J. Hegarty (2006), Satellite signal acquisition, tracking, and data demodulation, in *Understanding GPS - Principles and Applications*, chap. 5, edited by E. D. Kaplan and C. J. Hegarty, pp. 153–241, Artech House, Norwood, Mass.

Woo, K. T. (1999), Optimum semicodeless carrier phase tracking of L2, in 12th International Technical Meeting of the Satellite Division of the Institute of Navigation, Nashville, Tenn.

Yacoub, M. D. (2002), The α-μ distribution: A general fading distribution, Proc. 13th International Symposium on Personal, Indoor and Mobile Radio Communications, Lisbon, Portugal.

Yacoub, M. D. (2007), The α-μ distribution: A physical fading model for the Stacy distribution, *IEEE Trans. Veh. Technol.*, *56*, 27–24, doi:10.1109/TVT.2006.883753.

Yang, L., Z. Elmas, C. Hill, M. Aquino, and T. Moore (2011), An innovative approach for atmospheric error mitigation using new GNSS signals, *J. Navig.*, *64*, 211–232, doi:10.1017/S0373463311000373.

Yeh, K. C., and C. H. Liu (1982), Radio wave scintillations in the ionosphere, *Proc. IEEE*, *70*(4), 324–360, doi:10.1109/PROC.1982.12313.